Available online at www.sciencedirect.com

ScienceDirect

IFAC PapersOnLine CONFERENCE PAPER ARCHIVE

IFAC PapersOnLine 55-23 (2022) 68–73

Collagen Deposition in Diabetic Kidney Disease Boosts Intercellular Signaling: A Mathematical Model ⋆

Haryana Y. Thomas *,** **Ashlee N. Ford Versypt** *,**

* *School of Chemical Engineering, Oklahoma State University, Stillwater, OK 74078 USA*

** *Department of Chemical and Biological Engineering, University at Buffalo, The State University of New York, Buffalo, NY 14260 USA (email: ashleefv@buffalo.edu)*

Abstract: Diabetic kidney disease is a growing health burden. The limited options for treating and preventing diabetic kidney disease are in part due to gaps in our understanding of the progression of diabetic kidney damage and its impacts on cellular function. An important cellular function in the kidney glomerulus is intercellular communication via the release and uptake of soluble cytokines and growth factors. In diabetic kidney disease, excess collagen deposition alters the mesangial matrix properties, which, we hypothesized diminishes the intercellular signaling between key glomerular cells. To test our hypothesis, we combined established theoretical models of transport to study the impact of pathological deposition on the ability of cells to communicate via intercellular signaling. Our analysis reveals that pathological collagen deposition can enhance rather than diminish the signaling range of the glomerular cells.

Keywords: Cellular systems, physiological model, biomedical system modeling, simulation and visualization, kinetic modeling, and control of biological systems.

1. INTRODUCTION

Diabetes is a significant burden on public health. In about one-third of patients, diabetes leads to the severe complication diabetic kidney disease (DKD), which is the leading cause of kidney failure (Jitraknatee et al., 2020). Our lack of understanding of how DKD progresses and affects cellular and tissue function has contributed to our inability to mitigate the rapidly rising burden of DKD. Characterized by the presence of protein in the urin and a loss in glomerular filtration rate, DKD is induced by biochemical perturbations and morphological changes such as excess collagen deposition in the kidney's glomerular mesangium (Ban and Twigg, 2008; Mason and Wahab, 2003). The glomerular mesangium is a collagenous matrix that is located at the center of the glomerulus, the filtration unit of the kidney. The mesangium separates three key glomerular cell types: mesangial, endothelial, and podocyte cells. These cells are in constant communication in health and disease (Schlöndorff and Banas, 2009; Daehn, 2018). During DKD, cell-cell communication within the glomerular mesangium is affected by tissue damage. Elimination of PDGF-β, a key signaling molecule between mesangial and endothelial cells, has been shown to cause the development of an abnormal glomerulus (Levéen et al., 1994). This finding has been corroborated by multiple studies (Lindahl et al., 1998; Soriano, 1994; Bjarnegård et al., 2004). Additionally, inhibition of signaling pathways that mediate crosstalk between glomerular cells have been shown to ameliorate glomerular diseases (Johnson et al., 1992; Flyvbjerg et al., 2002). Consequently, interference in the signaling between glomerular cells has an impact on the function of the glomerulus in both health and disease. Interference in glomerular cell signaling occurs during diabetic kidney damage when the ability of signaling molecules to traverse through the mesangium is altered by excess collagen deposited in the mesangium. The extent to which the collagen deposition impacts intercellular signaling between glomerular cells has not been previously investigated computationally. We hypothesize that the pathological deposition of collagen blocks the path of signaling molecules and thus decreases the ability of glomerular cells to communicate.

In this work, we combined a theoretical intercellular transport model (Francis and Palsson, 1997) and a correlation for hindered diffusion in hydrogels (Amsden, 1998; Hunt et al., 2015) to study the impact of pathological collagen deposition on the effective signaling distance of a mesangial cell. We find from our quantitative study the surprising result that pathological collagen deposition can actually enhance the ability of cells to communicate rather than diminishing their ability to communicate.

⋆ This material is based upon work supported by the National Science Foundation under Grant No. 1845117/2133411 and resources from Oklahoma State University and the University at Buffalo. A preliminary version of this work, doi: https://doi.org/10.1101/2021.03.25.437068, was deposited in bioRxiv.

10.1016/j.ifacol.2023.01.017

2. METHODS

Here, we consider a single mesangial cell secreting signaling molecules that diffuse radially outward from the cell surface into the extracellular matrix. A one dimensional, spherical mass balance equation

$$\frac{\partial c}{\partial t} = D\frac{1}{r^2}\frac{\partial}{\partial r}\left[r^2\frac{\partial c}{\partial r}\right] \tag{1}$$

captures the temporal and spatial dynamics of the diffusing signaling molecules, where c represents the concentration of the signaling molecules, D represents the diffusion coefficient for signaling molecules diffusing through the matrix, r represents the radial distance from the center of the cell, and t represents time. The cell is assumed to be a spherical object of radius, ρ, residing in an isotropic matrix. We recognize that D will change slowly over the course of mesangial fibrosis in DKD, but D is assumed to have spatially uniform values that are constant at snapshots in time along the trajectory of chronic disease progression, which is much slower than the time scales for intercellular signaling and transport studied here.

The distribution of the signaling molecules through the matrix is dependent on physiologically relevant initial conditions and boundary conditions. These initial and boundary conditions are summarized below and are the same as those applied by Francis and Palsson (1997). The first boundary condition prescribes a constant flux

$$-D\frac{\partial c}{\partial r} = F_o \quad \text{at} \quad r = \rho, \tag{2}$$

where F_o is a constant secretion rate at the cell surface. The second boundary condition is

$$c \to 0 \quad \text{as} \quad r \to \infty. \tag{3}$$

We specify that initially no signaling molecules are present in the matrix:

$$c(r, 0) = 0. \tag{4}$$

Given these conditions, an analytical solution that describes the concentration profile of the signaling molecules in time and space can be obtained Francis and Palsson (1997)

$$\begin{aligned} c(r,t) =& \frac{F_o\rho}{D}\psi(r,t) \\ =& \frac{F_o\rho}{2Dr}\sqrt{\frac{4Dt}{\pi}}\left[\exp\left(\frac{-(r-\rho)^2}{4Dt}\right)\right. \\ & - \exp\left(\frac{-(r+\rho)^2}{4Dt}\right) \\ & \frac{-|r-\rho|}{\sqrt{\frac{4Dt}{\pi}}}\operatorname{erfc}\left(\left(\frac{|r-\rho|}{\sqrt{4Dt}}\right)\right) \\ & \left.+\frac{(r+\rho)}{\sqrt{\frac{4Dt}{\pi}}}\operatorname{erfc}\left(\left(\frac{(r+\rho)}{\sqrt{4Dt}}\right)\right)\right] \end{aligned} \tag{5}$$

where the key parameters are F_o, D, and ρ.

The effective signaling distance is obtained by finding the steady state propagation distance of the threshold concentration, k_m, which is the minimum concentration required to induce a response in a receiving cell located at that distance from the cell that secretes the signaling molecules. The propagation of the threshold concentration over time can be tracked by solving c/k_m for r. The steady state distance propagated by the threshold concentration can be found by taking the limit

$$\lim_{t\to\infty}\frac{c}{k_m} = \lim_{t\to\infty}\frac{F_o\rho}{Dk_m}\psi(r,t) = \frac{F_o\rho}{Dk_m}\frac{1}{r_{ss}}. \tag{6}$$

The steady state distance r_{ss} when $c = k_m$ is

$$r_{ss} = \frac{F_o\rho}{Dk_m}, \tag{7}$$

and we define the effective signaling distance (ESD) to be r_{ss}/ρ. Francis and Palsson (1997) defined the ESD to be half the maximum propagation distance because it took over 10^8 seconds to reach steady state in their scenario, which is an unrealistically long time scale for intercellular communication. In contrast, we define the effective signaling distance at the steady state distance because this steady state value is attained is less time for our case due to the smaller secretion rate of mesangial cells in comparison to the hybridoma cells studied by Francis and Palsson (1997). Since the ESD is dependent on diffusivity (7), we use it to study how changes in diffusivity of signaling molecules through the remodeling matrix impacts the ESD.

The diffusivity of signaling molecules is dependent on the properties of the matrix and the signaling molecules. We combine the equations above with a correlation for the diffusion coefficient through polymer hydrogels composed of rigid fibers (Amsden, 1998) to model the diffusivity of signaling molecules through the mesangial matrix. The mesangial matrix is composed of collagen fibers and other soluble chemicals. Hydrogels are commonly used to mimic the properties of the extracellular matrix in many tissues (Kyburz and Anseth, 2015). The correlation takes into account the hydrodynamic drag and obstruction effects of matrix fibers on solute molecule diffusivity (Amsden, 1998), and it has been previously used to capture the variations of solute diffusivity through the extracellular matrix of the mesangium (Hunt et al., 2015). The matrix is modeled as a fibrous mesh with a physiologically relevant porosity represented by volume fraction occupied by the fibers, ϕ, and average fiber radius, r_f. Collagen deposition is assumed to change the porosity of the matrix, which in turn changes the effective diffusion coefficient D via the relationship (Amsden, 1998)

$$D = D_o\exp(-\pi\phi^b)\exp(-0.84f^{1.09}). \tag{8}$$

D_o is the free diffusion coefficient given by the Stokes-Einstein equation

$$D_o = \frac{k_BT}{6\pi\mu r_s}, \tag{9}$$

where k_B is Boltzmann's constant, T is the temperature, and μ is the viscosity of interstitial fluid, which we assume to have the same viscosity as blood plasma. The following functions define the terms b and f in (8):

$$b = 0.174\ln\left(\frac{59.6}{\lambda}\right) \tag{10}$$

$$f = (1+\lambda^2)\phi \tag{11}$$

where λ is the the ratio of the solute radius, r_s, to the fiber radius, r_f.

Model parameters were obtained from previous papers that modeled transport through the mesangial matrix and

are listed in Table 1. In cases where exact parameters values were unavailable, we found general expected ranges. For instance, mesangial cell cytokine secretion rates are not readily available in the literature because quantification of secretion rates is difficult (Gao et al., 2014; Frykman and Srienc, 1998) and the methods are still being refined (Juan-Colas et al., 2018; Gao et al., 2014; Raphael et al., 2013; Han et al., 2010; Zhou et al., 2020). For short range signaling cells, however, cytokine secretion rates are estimated to be on the order of 10–100 molecules/cell/s (Kwa et al., 2014; Jansson et al., 2007; Han et al., 2010). Threshold concentrations also vary widely but are estimated to be on the order of 10–50 pM (Francis and Palsson, 1997). We chose the upper end of the secretion rates and lower end of the threshold concentration to obtain the upper limit of the signaling ranges. Collagen volume fractions in kidney fibrosis as well as fibrosis in other tissues is on the order of 0.05 to 0.30 (Shen et al., 2008; Yu et al., 1998; Barsky et al., 1982). A majority of cytokines and growth factors have molecular weights that are on the order of 10–60 kDa (Ott et al., 2018; Helmy et al., 2009), which approximates to hydrodynamic radii of 2–6 nm.

The model equations were solved using MATLAB version R2020b. We made the MATLAB code used for the calculations available in our online repository (Thomas and Ford Versypt, 2021).

Table 1. List of parameters used in the model.

Symbol	Value
r_f	10–20 nm (Hunt et al., 2015)
r_s	2–6 nm
ϕ	0.05–0.15 (Hunt et al., 2015)
F_o	100 molecules cell^{-1} s^{-1}
ρ	5 μm (Hunt et al., 2015; Dubus et al., 2002)
k_m	10 pM (Francis and Palsson, 1997)
μ	7×10^{-4} Pa·s (Hunt et al., 2015)

3. RESULTS AND DISCUSSION

Using the parameters listed in Table 1, we obtained concentration profiles of the signaling molecule through the matrix over time until 10^8 seconds, a period long enough for steady state to be achieved (Fig. 1a). Over time, as expected, signaling molecules begin to accumulate as the cell continues to secrete. More importantly, as the time progresses the accumulation rate of signaling molecules decreases and approaches a steady state value of around two and a half times the threshold concentration at the cell surface (Fig. 1a). This approach to steady state is more clearly observed in Fig. 1b, which shows the propagation of the threshold concentration through the spatial domain over time. We observe a significant propagation over the first 10^3 seconds that plateaus to reach $r_{ss} \approx 0.001$ cm at 10^4 seconds (Fig. 1b). Consequently, even if the cell continues secreting for a longer period of time, the threshold concentration could not propagate any farther.

The impact of collagen deposition on the effective diffusion coefficient for different sized signaling molecules has been plotted in Fig. 2 using physiologically relevant values.

The model shows a significant exponential decay relationship between the volume fraction and the effective diffusion coefficient (Fig. 2). For pathological changes in fiber radius, the increase in the effective diffusion coefficient is small (Fig. 2). Thus, the dependence of the effective diffusion coefficient on the fiber radius is weak relative to the dependence of the effective diffusion coefficient on the volume fraction.

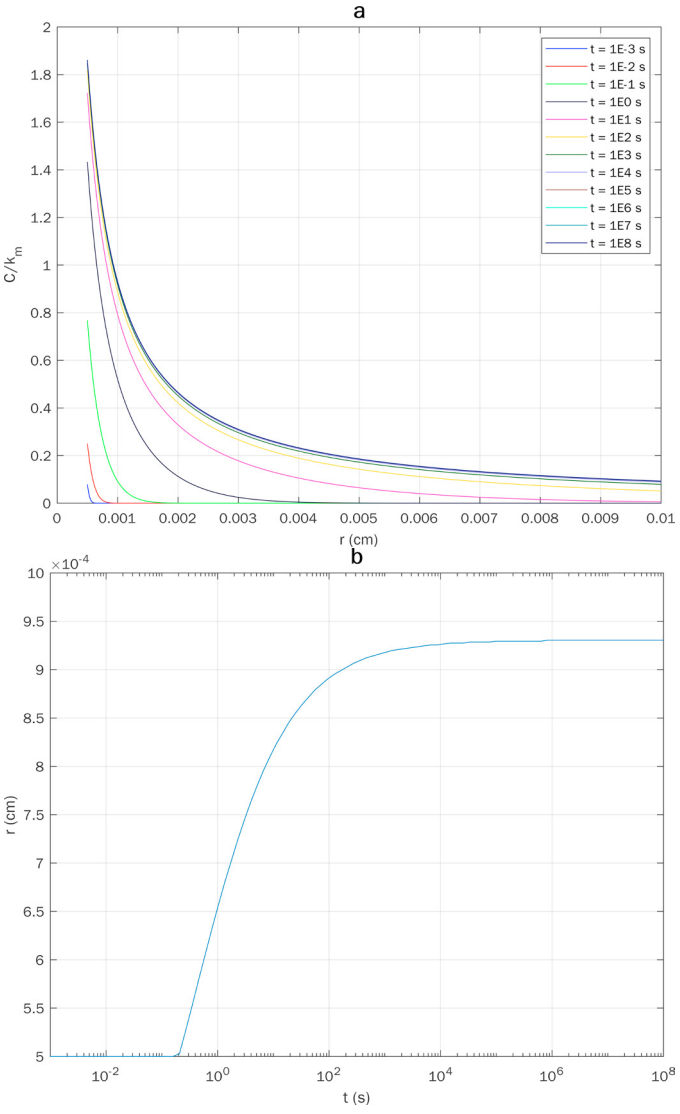

Fig. 1. (a) Concentration profile of secreted signaling molecules obtained from analytical solution. Concentration is scaled by the threshold concentration. (b) Propagation distance of the threshold concentration of signaling molecules over time. Base case: $\phi = 0.05$, $r_s = 2$ nm, and $r_f = 20$ nm.

The ESDs for healthy, moderately diseased, and severely diseased matrices for different sized signaling molecules is shown in Fig. 3 and represented by the green ($\phi = 0.05$), yellow ($\phi = 0.10$), and red ($\phi = 0.15$) curves, respectively. As the matrix becomes diseased due to collagen deposition, the ESD increases from an initial signaling distance of 2.5 cell radii to approximately 5 cell radii for small molecules and to over 10 cell radii for large signaling molecules (Fig. 3). This is surprising, because we had hypothesized that as the matrix becomes diseased, the ability of cells to signal would decrease. However, we see from these results that

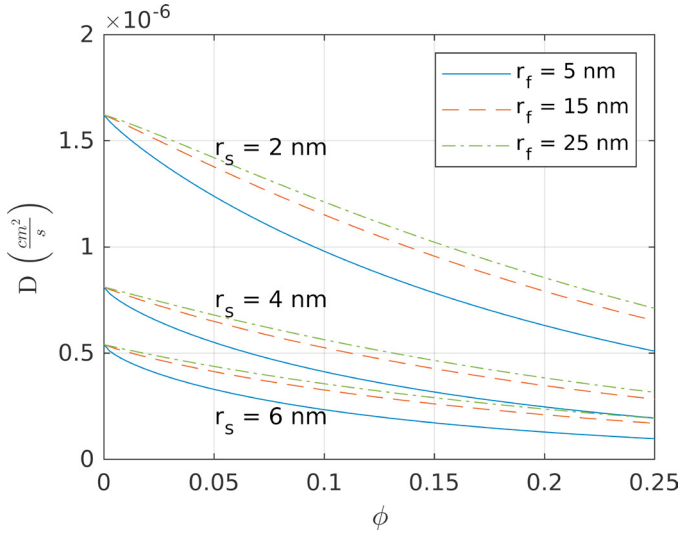

Fig. 2. Collagen deposition decreases the diffusivity of signaling molecules. Effective diffusion coefficient D as a function of the matrix volume fraction ϕ, solute radius r_s, and fiber radius r_f.

a diseased matrix actually enhances the ability of a cell to signal rather than diminishing it. Additionally, larger signaling molecules have greater signaling distances than smaller signaling molecules, and the signaling distance of large molecules is further increased in diseased conditions (Fig. 3).

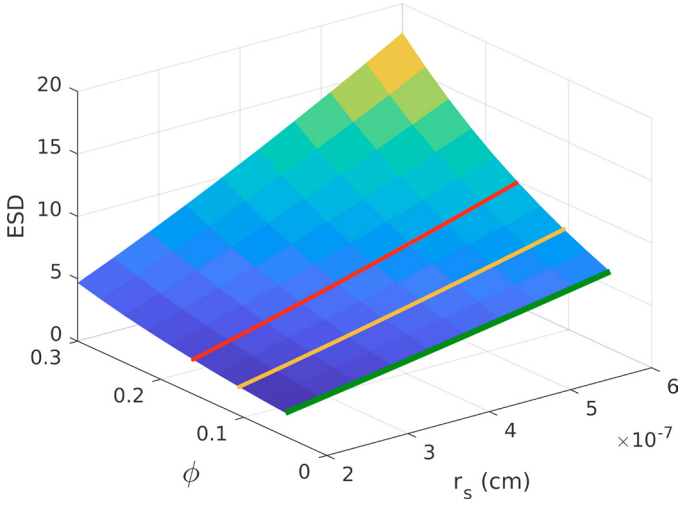

Fig. 3. Effective signaling distances (ESD) for secreted signaling molecules increases as collagen deposition increases. Green, yellow, and red curves represent healthy, moderately diseased, and diseased matrices, respectively. Matrix volume fraction of up to 0.3 is shown to emphasize the nonlinear increasing trend. Results obtained using parameter values listed in Table 1 and $r_f = 20$ nm.

Compared to previous findings, our predicted values for the ESD in the healthy case are in the right magnitude. Using experimental and computational methods, Bagnall et al. estimated that the signaling distance for macrophages is on the order of a few cell diameters (Bagnall et al., 2018), a result that has been shown to be the case for T cells as well (Thurley et al., 2015). Our model predicts a signaling distance of 1–3 cell diameters (2–5 cell radii) for the healthy case, but this is an overestimate because we do not incorporate signaling molecule uptake by neighboring cells, which has been taken into account by the other studies. We also neglect convective transport of signaling molecules, which would theoretically increase the signaling distance. Although we cannot specify the extent to which each assumption impacts the ESD, their opposing influence on ESD could nullify any individual impact. Regardless, this is a potential area for future work.

Our predictions regarding the changes in ESD due to collagen deposition in the mesangium, however, cannot be compared to experimental data because such data is not yet available. However, the trend that is observed of an increase in propagation distance due to a decrease in diffusivity is a phenomenon that has been previously described in general (Lander, 2007; Saha and Schaffer, 2006; Jansson et al., 2007). Additionally, other modeling studies that consider the uptake of signaling molecules show that the trend is still observed (Frykman and Srienc, 1998). The unexpected increase in signaling distance occurs because the decline in the diffusivity of signaling molecules results in an increased accumulation of signaling molecules at the surface of the cell, which creates a steep gradient leading to a larger propagation distance of the signaling molecules. In our model, this behavior is governed by the boundary condition at the surface of the cell (2), which states that the concentration gradient at the cell surface is equal to the secretion rate divided by the diffusion coefficient. Although this modeling strategy has been implemented previously (Francis and Palsson, 1997; Frykman and Srienc, 1998), it still needs to be experimentally validated.

Although signaling distance increases with a decrease in diffusivity under both physiological and pathophysiological parameter ranges, there are also cases where signaling distance decreases with a decrease in diffusivity (Fig. 4). Concentration profiles of signaling molecules at two diffusion coefficients, representative of matrices with different transport properties and at four separate time points have been plotted (Fig. 4). The results show that there are points on the concentration curves, at time 10 s and 100 s, where the higher diffusion coefficient has propagated farther than the concentration curve with the lower diffusion coefficient. However, that is only observed for a short time (Fig. 4). As steady state is approached the lower diffusion coefficient propagates further. This behavior is dependent on secretion rate and threshold concentration and has been previously observed theoretically in other biological applications (Lander, 2007; Saha and Schaffer, 2006).

In conclusion, we elucidated the impact of pathological collagen deposition in the mesangial matrix on intercellular communication. Contrary to our hypothesis, we found that as the level of collagen deposition increases, the signaling range of the mesangial cell increases and that the increase is amplified for large signaling molecules. This finding has implications because an increase in signaling range can result in the propagation of a signal to unintended cells. For example, a profibrotic signal that is normally constrained to immediate neighbors may propagate to non-neighboring cells to stimulate pathological collagen

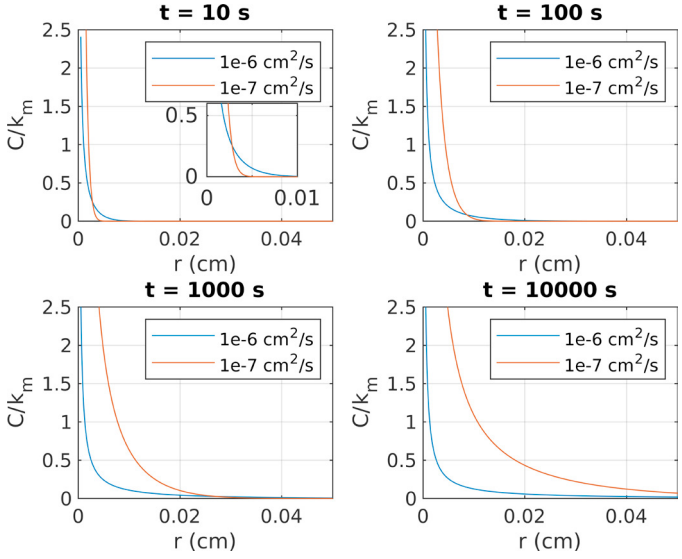

Fig. 4. Scenarios where propagation distance of signaling molecules can be reduced for lower diffusivity. $D = 1\times 10^{-6}\text{cm}^2/\text{s}$ represents higher diffusivity, and $D = 1 \times 10^{-7}\text{cm}^2/\text{s}$ represents a lower diffusivity.

deposition. This process creates a positive feedback loop between signaling and collagen deposition that then exacerbates disease condition. Our analysis here shows that pathological collagen deposition disrupts the controlled localized signaling of cells, which then contributes to the exacerbation of diabetic kidney damage. This may also hold in other fibrotic diseases.

REFERENCES

Amsden, B. (1998). Solute diffusion within hydrogels. Mechanisms and models. *Macromolecules*, 31(23), 8382–8395.

Bagnall, J., Boddington, C., England, H., Brignall, R., Downton, P., Alsoufi, Z., Boyd, J., Rowe, W., Bennett, A., Walker, C., Adamson, A., Patel, N.M., O'Cualain, R., Schmidt, L., Spiller, D.G., Jackson, D.A., Mller, W., Muldoon, M., White, M.R., and Paszek, P. (2018). Quantitative analysis of competitive cytokine signaling predicts tissue thresholds for the propagation of macrophage activation. *Science Signaling*, 11(540), aaf3998.

Ban, C.R. and Twigg, S.M. (2008). Fibrosis in diabetes complications: pathogenic mechanisms and circulating and urinary markers. *Vascular Health and Risk Management*, 4(3), 575–96.

Barsky, S.H., Rao, C.N., Grotendorst, G.R., and Liotta, L.A. (1982). Increased content of type V collagen in desmoplasia of human breast carcinoma. *American Journal of Pathology*, 108(3), 276–283.

Bjarnegård, M., Enge, M., Norlin, J., Gustafsdottir, S., Fredriksson, S., Abramsson, A., Takemoto, M., Gustafsson, E., Fässler, R., and Betsholtz, C. (2004). Endothelium-specific ablation of PDGFβ leads to pericyte loss and glomerular, cardiac and placental abnormalities. 131(8), 1847–1857.

Daehn, I.S. (2018). Glomerular endothelial cell stress and cross-talk with podocytes in early diabetic kidney disease. *Frontiers in Medicine*, 5, 76.

Dubus, I., Vendrely, B., Christophe, I., Labouyrie, J.P., Delmas, Y., Bonnet, J., and Combe, C. (2002). Mycophenolic acid antagonizes the activation of cultured human mesangial cells. *Kidney International*, 62(3), 857–867.

Flyvbjerg, A., Dagnæs-Hansen, F., De Vriese, A.S., Schrijvers, B.F., Tilton, R.G., and Rasch, R. (2002). Amelioration of long-term renal changes in obese type 2 diabetic mice by a neutralizing vascular endothelial growth factor antibody. *Diabetes*, 51(10), 3090–3094.

Francis, K. and Palsson, B.O. (1997). Effective intercellular communication distances are determined by the relative time constants for cyto/chemokine secretion and diffusion. *Proceedings of the National Academy of Sciences*, 94(23), 12258–12262.

Frykman, S. and Srienc, F. (1998). Quantitating secretion rates of individual cells: Design of secretion assays. *Biotechnology and Bioengineering*, 59(2), 214–226.

Gao, Y., Zhou, Q., Matharu, Z., Liu, Y., Kwa, T., and Revzin, A. (2014). A mathematical method for extracting cell secretion rate from affinity biosensors continuously monitoring cell activity. *Biomicrofluidics*, 8(2), 4874216.

Han, Q., Bradshaw, E.M., Nilsson, B., Hafler, D.A., and Love, J.C. (2010). Multidimensional analysis of the frequencies and rates of cytokine secretion from single cells by quantitative microengraving. *Lab on a Chip*, 10(11), 1391–1400.

Helmy, A., Carpenter, K.L., Skepper, J.N., Kirkpatrick, P.J., Pickard, J.D., and Hutchinson, P.J. (2009). Microdialysis of cytokines: Methodological considerations, scanning electron microscopy, and determination of relative recovery. *Journal of Neurotrauma*, 26(4), 549–561.

Hunt, S.E., Dorfman, K.D., Segal, Y., and Barocas, V.H. (2015). A computational model of flow and species transport in the mesangium. *American Journal of Physiology - Renal Physiology*, 310, 222–229.

Jansson, A., Harlen, M., Karlsson, S., Nilsson, P., and Cooley, M. (2007). 3D computation modelling of the influence of cytokine secretion on Th-cell development suggests that negative selection (inhibition of Th1 cells) is more effective than positive selection by IL-4 for Th2 cell dominance. *Immunology and Cell Biology*, 85(3), 189–196.

Jitraknatee, J., Ruengorn, C., and Nochaiwong, S. (2020). Prevalence and risk factors of chronic kidney disease among type 2 diabetes patients: a cross-sectional study in primary care practice. *Scientific Reports*, 10(1), 1–10.

Johnson, R.J., Raines, E.W., Floege, J., Yoshimura, A., Pritzl, P., Alpers, C., and Ross, R. (1992). Inhibition of mesangial cell proliferation and matrix expansion in glomerulonephritis in the rat by antibody to platelet-derived growth factor. *Journal of Experimental Medicine*, 175(5), 1413–1416.

Juan-Colas, J., Hitchcock, I.S., Coles, M., Johnson, S., and Krauss, T.F. (2018). Quantifying single-cell secretion in real time using resonant hyperspectral imaging. *Proceedings of the National Academy of Sciences*, 115(52), 13204–13209.

Kwa, T., Zhou, Q., Gao, Y., Rahimian, A., Kwon, L., Liu, Y., and Revzin, A. (2014). Reconfigurable microfluidics with integrated aptasensors for monitoring intercellular communication. *Lab on a Chip*, 14(10), 1695–1704.

Kyburz, K.A. and Anseth, K.A. (2015). Synthetic mimics of the extracellular matrix: how simple is complex enough? *Annals of Biomedical Engineering*, 43(3), 489–500.

Lander, A.D. (2007). Morpheus unbound: reimagining the morphogen gradient. *Cell*, 128(2), 245–256.

Levéen, P., Pekny, M., Gebre-Medhin, S., Swolin, B., Larsson, E., and Betsholtz, C. (1994). Mice deficient for PDGF-β show renal, cardiovascular, and hematological abnormalities. *Genes and Development*, 8(16), 1875–1887.

Lindahl, P., Hellström, M., Kalén, M., Karlsson, L., Pekny, M., Pekna, M., Soriano, P., and Betsholtz, C. (1998). Paracrine PDGF-β/PDGF-Rβ signaling controls mesangial cell development in kidney glomeruli. *Development*, 125(17), 3313–3322.

Mason, R.M. and Wahab, N.A. (2003). Extracellular matrix metabolism in diabetic nephropathy. *Journal of the American Society of Nephrology*, 14(5), 1358–1373.

Ott, B.R., Jones, R.N., Daiello, L.A., de la Monte, S.M., Stopa, E.G., Johanson, C.E., Denby, C., and Grammas, P. (2018). Blood-cerebrospinal fluid barrier gradients in mild cognitive impairment and Alzheimer's disease: Relationship to inflammatory cytokines and chemokines. *Frontiers in Aging Neuroscience*, 10, 00245.

Raphael, M.P., Christodoulides, J.A., Delehanty, J.B., Long, J.P., and Byers, J.M. (2013). Quantitative imaging of protein secretions from single cells in real time. *Biophysical Journal*, 105(3), 602–608.

Saha, K. and Schaffer, D.V. (2006). Signal dynamics in Sonic hedgehog tissue patterning. *Development*, 133(5), 889–900.

Schlöndorff, D. and Banas, B. (2009). The mesangial cell revisited: No cell is an island. *Journal of the American Society of Nephrology*, 20(6), 1179–1187.

Shen, B., Hagiwara, M., Yao, Y.Y., Chao, L., and Chao, J. (2008). Salutary effect of kallistatin in salt-induced renal injury, inflammation, and fibrosis via antioxidative stress. *Hypertension*, 51(5), 1358–1365.

Soriano, P. (1994). Abnormal kidney development and hematological disorders in PDGF β- receptor mutant mice. *Genes and Development*, 8(16), 1888–1896.

Thomas, H.Y. and Ford Versypt, A.N. (2021). *ColDepSignalingImpact*. http://github.com/ashleefv/ColDepSignalingImpact.

Thurley, K., Gerecht, D., Friedmann, E., and Höfer, T. (2015). Three-dimensional gradients of cytokine signaling between T cells. *PLoS Computational Biology*, 11(4), 1004206.

Yu, H.C., Burrell, L.M., Black, M.J., Wu, L.L., Dilley, R.J., Cooper, M.E., and Johnston, C.I. (1998). Salt induces myocardial and renal fibrosis in normotensive and hypertensive rats. *Circulation*, 98(23), 2621–2628.

Zhou, L., Chen, P., and Simonian, A. (2020). Advanced Biosensing towards Real-Time Imaging of Protein Secretion from Single Cells. In *Biosensor - Current and Novel Strategies for Biosensing*. IntechOpen.